Hydrophobic Coupling of Lipid Bilayer Energetics to Channel Function

Robyn L. Goforth,[1] Aung K. Chi,[2] Denise V. Greathouse,[1] Lyndon L. Providence,[2] Roger E. Koeppe II,[1] and Olaf S. Andersen[2]

[1]Department of Chemistry and Biochemistry, University of Arkansas, Fayetteville, AR 72701

[2]Department of Physiology and Biophysics, Weill Medical College of Cornell University, New York, NY 10021

ABSTRACT The hydrophobic coupling between membrane-spanning proteins and the lipid bilayer core causes the bilayer thickness to vary locally as proteins and other "defects" are embedded in the bilayer. These bilayer deformations incur an energetic cost that, in principle, could couple membrane proteins to each other, causing them to associate in the plane of the membrane and thereby coupling them functionally. We demonstrate the existence of such bilayer-mediated coupling at the single-molecule level using single-barreled as well as double-barreled gramicidin channels in which two gramicidin subunits are covalently linked by a water-soluble, flexible linker. When a covalently attached pair of gramicidin subunits associates with a second attached pair to form a double-barreled channel, the lifetime of both channels in the assembly increases from hundreds of milliseconds to a hundred seconds—and the conductance of each channel in the side-by-side pair is almost 10% higher than the conductance of the corresponding single-barreled channels. The double-barreled channels are stabilized some 100,000-fold relative to their single-barreled counterparts. This stabilization arises from: first, the local increase in monomer concentration around a single-barreled channel formed by two covalently linked gramicidins, which increases the rate of double-barreled channel formation; and second, from the increased lifetime of the double-barreled channels. The latter result suggests that the two barrels of the construct associate laterally. The underlying cause for this lateral association most likely is the bilayer deformation energy associated with channel formation. More generally, the results suggest that the mechanical properties of the host bilayer may cause the kinetics of membrane protein conformational transitions to depend on the conformational states of the neighboring proteins.

KEY WORDS: gramicidin channels • bilayer mechanics • hydrophobic coupling • lateral association

INTRODUCTION

Ion channels and other integral membrane proteins often are distributed nonrandomly in biological membranes (Lester, 1977; Almers and Stirling, 1984; Poo, 1985; Harris, 2001). This lateral organization can couple functionally different channel types (Roberts et al., 1990; Issa and Hudspeth, 1994) and protein clustering can alter protein function (Young and Poo, 1983; Iwasa et al., 1986). The lateral heterogeneity in cell membranes pertains not only to the protein but also the lipid component (Simons and Ikonen, 1997; Mouritsen and Andersen, 1998). Moreover, disruptions in the membrane bilayer lipid composition alter the (re)distribution of protein components (Chang et al., 1995) and clustering of proteins alters their distribution between different bilayer components (Tkachenko and Simons, 2002), but it remains unclear whether the changes in protein function that occur during a redistribution of membrane proteins (Young and Poo, 1983) are the primary result of direct protein–protein interactions or whether significant interactions also are transmitted through the bilayer.

Address editorial correspondence to Roger E. Koeppe II, Department of Chemistry and Biochemistry, University of Arkansas, Fayetteville, AR 72701. Fax: (479) 575-4049; E-mail: rk2@uark.edu

Integral membrane protein folding depends on the association of bilayer-spanning α-helices, which is due to more favorable helix–helix, as compared with helix–lipid, interactions (e.g., Popot and Engelman, 1990; Lemmon and Engelman, 1994; White and Wimley, 1999). The clustering of membrane proteins often is mediated by cytoskeletal proteins, such as the PDZ family of proteins (Fanning and Anderson, 1999). Similarly, extracellular ligand binding to growth factor receptors can induce receptor dimerization, which precedes the autophosphorylation that initiates the signal-transduction cascade (Ullrich and Schlessinger, 1990). The lipid bilayer component also can promote membrane protein clustering when there is a significant mismatch between the proteins' hydrophobic length and the thickness of the bilayer hydrophobic core (Kusumi and Hyde, 1982; Lewis and Engelman, 1983; Pearson et al., 1983; Cornea and Thomas, 1994). Similar changes in bilayer thickness also alter the function of imbedded proteins (Baldwin and Hubbell, 1985; Brown, 1994; Starling et al., 1995; Cornelius, 2001). In some cases, e.g., the sarcoplasmic Ca^{2+}-ATPase (Starling et al., 1995), the bilayer-dependent changes in protein function are not dependent on aggregation or clustering. In other cases, e.g., the nicotinic acetylcholine receptor (Young and Poo, 1983) and the cyclic lipodepsipeptide syringomycin E (Kaulin et al.,

1998), the changes in protein function result from the clustering itself; and in some cases of heterologously expressed ion channels, e.g., CFTR (Larsen et al., 1996), cooperative channel openings are suggestive of channel clustering. In yet other cases, e.g., the ryanodine receptor (Marx et al., 1998), the functional coupling (dimerization) is favored by the presence of an accessory protein FKBP12 but can occur even in its absence. It is not clear, however, whether clustering alters protein function because of protein–protein interactions or because of bilayer-mediated interactions. In fact, even though bilayer-mediated interactions between membrane proteins have been proposed (e.g., Young and Poo, 1983; Manivannan et al., 1992), there is little direct evidence for such interactions. Moreover, within the confines of the "standard" fluid-mosaic membrane model (Singer and Nicolson, 1972), which often is assumed to equate the bilayer with a thin sheet of liquid hydrocarbon, there is no obvious physical basis such for bilayer-mediated protein interactions.

Simply extending the fluid-mosaic model to incorporate the fact that lipid bilayers are elastic bodies with well-defined material properties (Evans and Hochmuth, 1978; Mouritsen and Bloom, 1984; Huang, 1986; Evans and Needham, 1987) provides a physical basis for such interactions. Because lipid bilayers are elastic bodies, a mismatch between a protein's hydrophobic length and the bilayer hydrophobic thickness will cause a local bilayer deformation. This deformation not only incurs an energetic cost, it also extends 2–3 nm into the surrounding bilayer (Aranda-Espinoza et al., 1996; Huang, 1986; Nielsen et al., 1998; Partenskii and Jordan, 2002), which could lead to protein clustering (Aranda-Espinoza et al., 1996; Harroun et al., 1999b). Experimental evidence for such a hydrophobic mismatch-driven clustering was, in fact, provided for gramicidin channels incorporated into bilayers of different thickness (Harroun et al., 1999a), but the functional significance of this clustering has not been established.

Gramicidin A (gA) from *Bacillus brevis* forms monovalent cation–selective channels in which each 15–amino-acid β-helical subunit is inserted in one of the lipid bilayer leaflets (Koeppe and Andersen, 1996; Andersen et al., 1999). Usually, the hydrophobic length of an assembled dimeric gramicidin channel is less than the host bilayer's hydrophobic thickness (Elliott et al., 1983), and the formation of a gA channel is expected to compress and bend the monolayers toward each other (Huang, 1986; Andersen et al., 1999; Nielsen and Andersen, 2000). This is indeed the case, as X-ray diffraction measurements show that the peak-to-peak distance in the electron density profile of dimyristoylphosphatidylcholine (DMPC)* bilayers decreases form 35.3 to 32.7 Å upon the incorporation of gA at a 1:10 gA/DMPC molar ratio (Harroun et al., 1999a). Moreover, the radial distribution function suggests that the bilayer-spanning gA channels tend to cluster. In dilute systems, the average thinning would be less, but the lipids near each embedded entity nevertheless could experience a similar relative deformation. This bilayer deformation, with its associated deformation energy, could provide the means for coupling two channels together. Moreover, given the structure of gramicidin channels, which are fully imbedded within the bilayer (Olah et al., 1991), any coupling between channels would be bilayer-mediated.

The aim of the present experiments therefore was to examine whether a local thinning of the lipid bilayer, caused by the formation of a gramicidin channel, could influence the properties (e.g., the channel formation rate, single-channel conductance, or lifetime) of a nearby channel? The typical single-channel experiment cannot answer this question because the systems are extremely dilute, one subunit per 10^6 or 10^7 lipid molecules (Durkin et al., 1990; Sawyer et al., 1990). To overcome this limitation, we joined two gA monomers via a flexible, hydrophilic extra-membrane peptide linker at their carboxy terminals. One anticipates that the pair of subunits of such a carboxy-linked dimer potentially could join with equivalent subunits from another linked dimer to facilitate side-by-side channel formation (Fig. 1).

Dimers were prepared by synthesizing two gA moieties that are connected via flexible peptide chains to a single lysine, using both the α- and ε-amino groups as attachment sites. In this article we show that double-barreled channels can be formed when the linkers are sufficiently long, and that these double-barreled channels are stabilized some two orders of magnitude relative to the single-barreled channels. In the accompanying article by Rokitskaya et al. (2003), the problem is addressed from the point of view of ligand-induced receptor dimerization—based on streptavidin-induced dimerization of biotin-labeled gramicidins. The results of these two studies are in general agreement, and suggest that bilayer-mediated protein interactions can be important for membrane protein function.

Some of these results have appeared in preliminary form (Goforth et al., 2002).

MATERIALS AND METHODS

Gramicidin Analogues

To separate the possible consequences of coupling an extended peptide segment to a gramicidin monomer, we synthesized ana-

*Abbreviations used in this paper: γ-Aba, γ-NH_2-butyric acid; eda, ethylene diamine; DMPC, dimyristoylphosphatidylcholine; DPhPC, diphytanoylphosphatidylcholine; gA, gramicidin A; MALDI, matrix-assisted laser desorption ionization; RP-HPLC, reversed phase high pressure liquid chromatography.

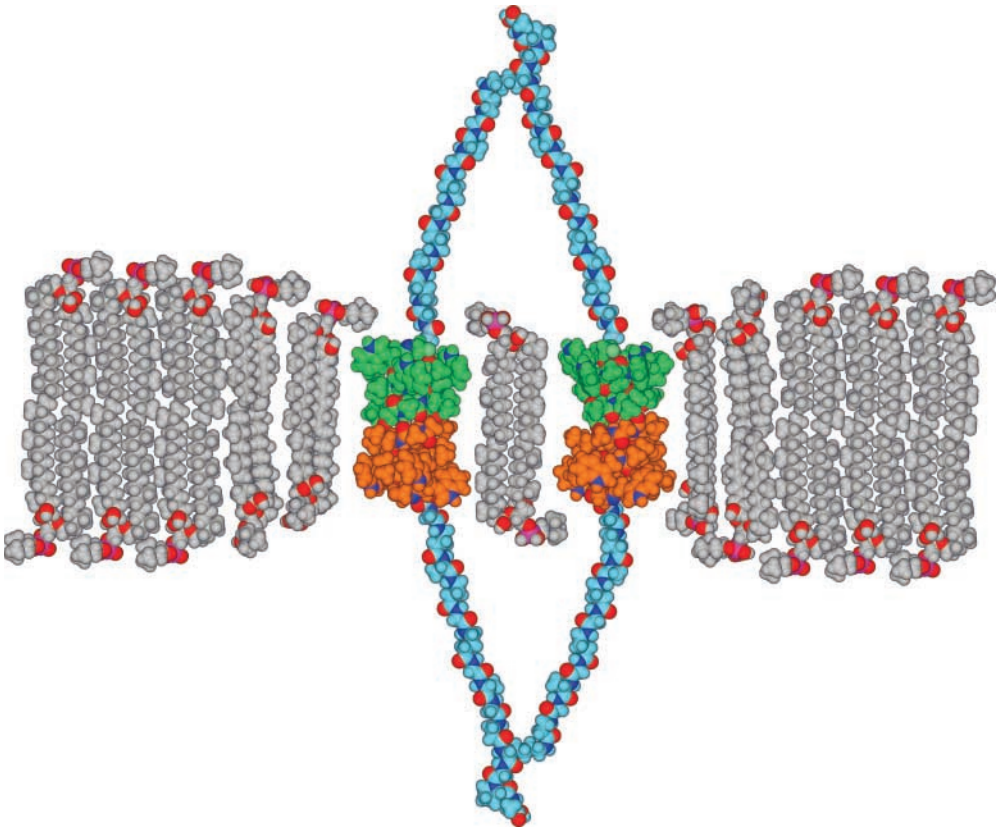

FIGURE 1. Schematic model of side-by-side, double-barreled gramicidin channels that assemble from two pairs of linked subunits in a lipid bilayer. Each individual subunit spans one leaflet of the DPhPC bilayer and is joined at its COOH-terminal to an adjacent subunit, in the same leaflet, by means of a hydrophilic peptide linker, which extends into the aqueous solution. The two peptide strands in the linker are joined by a lysine, which is extended by three more carboxy-terminal residues to further increase the linker's water solubility (and also were necessary for efficient synthesis). The flexible linkers are shown to scale in an arbitrary extended conformation. Channel formation requires that two subunits in opposite leaflets associate to form a hydrogen bond–stabilized cation-conducting channel. In a double-barreled channel, the two covalently linked subunits in one leaflet form bilayer-spanning channels with two covalently linked subunits in the opposite leaflet. The lipids distant from the channel barrels are represented as DPhPC molecules with fully extended acyl chains, which will tend to exaggerate the hydrophobic mismatch between the channel and the bilayer. To illustrate how the bilayer adapts to the bilayer-spanning channels, the lipids adjacent to or near a channel barrel are depicted with acyl chains that have been shortened by two carbons (second "shell") or four carbons (first "shell"), which represents the bilayer thinning. Carbon and hydrogen atom colors reflect the particular molecular components: gramicidin subunits, green/orange; lipids, gray; linkers, light blue. The colors for other atoms are: O, red; N, dark blue; P, magenta.

logues with single-ended tail sequences as well as linked gramicidin analogues. Further, in the linked gramicidins, the linker needs to be long enough to allow both channels to insert and move freely in the bilayer, yet short enough to keep the gramicidins in fairly close physical proximity within the bilayer. To this end, we designed flexible linker segments of two different lengths, in which the carboxy termini of two identical peptide segments are coupled to a common lysine and the segments' amino termini are coupled to the carboxyl residue of Trp^{15} in the gA sequence. The resulting linked gramicidins have linkers with 15 or 23 amino acids (including the bifunctional Lys), which were synthesized to bridge the Trp^{15} of one gA sequence to the Trp^{15} of another (Table I). The control single-ended tail sequences have 7 or 13 residues coupled to Trp^{15} of gA.

In all cases, the Trp^{15} was coupled to a γ-NH_2-butyric acid to minimize the possibility that the linker simply would serve to extend the $\beta^{6.3}$-helical gA structure. (Not only is the L-D chirality broken, in γ-NH_2-butyric acid there are two CH_2 moieties inserted between the CO and the C-NH.) Further, to maximize flexibility and length, and minimize the risk that the linkers have well-defined secondary structures, the linkers incorporate both β-Ala and γ-NH_2-butyric acid (γ-Aba) residues, which interrupt the secondary structure and further extend the backbone length with extra CH_2 groups. To ensure sufficient water solubility, the linkers were synthesized using amino acids with no more than two methylene units inserted between the carboxyl and amino groups. The effective length of the 15-residue linker, with 55 atoms in the backbone, is therefore equivalent to that of an 18-residue peptide; and the effective length of the 23-residue linker, with 91 atoms in the backbone, is equivalent to that of a 30-residue peptide. The lengths of the stretched-out linkers therefore will be ~8 and 14 nm, respectively, which means that the (local) molar ratio of gramicidin subunits to phospholipids will be ~1/300 and 1/900—three-to-four orders of magnitude higher than normally used in single-channel studies (Durkin et al., 1990).

The analogues with single-ended tails were synthesized and purified using standard solid-phase procedures (Greathouse et al., 1999).

The linked analogues were synthesized by the addition of Fmoc-protected amino acids to a low-loaded (0.25 mmole/g) Sasrin®-Ala resin (Mergler et al., 1988). For these analogues, the synthetic procedures were modified from those used for the analogues with single-ended tails, so as to allow for 30–50 min deprotection times and 12 h coupling times using a 25-fold excess of the incoming Fmoc amino acid. To minimize unwanted side reactions, each coupling was followed by extensive wash cycles and extra solvation volumes. As a critical step in the synthesis, the bifunctional Lys, denoted K* in Table I, was coupled to the resin after a COOH-terminal Gly-Pro-Ala sequence. This "spacer" was necessary for efficient formation of both of the peptide chains that grew out from the bifunctional Lys. This coupling sequence serves no other purpose in terms of channel formation or chan-

TABLE I

Sequences of the Gramicidins Used in this Study

gA	f-V-G-A-L-A-V-V-V-W-L-W-L-W-L-W-ea
gA with 7-residue eda tail	(gA)-γAba-G-A-G-A-G-A-eda
gA with 7-residue ea tail	(gA)-γAba-G-A-G-A-G-A-ea
gA with 13-residue ea tail	(gA)-γAba-G-A-G-A-G-A-γAba-G-A-N-G-A-ea
15-residue-linked tandem gA	[(gA)-γAba-G-A-G-A-G-βAla]$_2$-K*-G-P-A
23-residue-linked tandem gA	[(gA)-γAba-G-γAba-A-γAba-G-γAba-G-A-G-βAla]$_2$-K*-G-P-A

The underlined residues are D-amino acids. f, formyl; ea, ethanolamide; eda, ethylene diamine; γAba, γ-aminobutyric acid; βAla, β-alanine. The ethanolamide in gA is absent in the analogues with single-ended tails or linkers, as each W^{15} is attached to the first γAba of the tail or linker.

nel connections. The bifunctional di-Fmoc-lysine (K*), which constitutes the actual link, was dually deprotected and derivatized at both the α- and ε-amino groups, such that both amino groups could be used as starting points for the synthesis of an identical linker-gA sequence. The resulting peptide products were released from the Sasrin® resin using 1% trifluoroacetic acid in dichloromethane for 3 min at 24°C and purified by reversed phase high pressure liquid chromatography (RP-HPLC) on a Zorbax C-8 Column (Greathouse et al., 1999). The linked analogues were eluted as a single broad peak using a gradient of 80–99% methanol (and 20–1% water) with 0.1% trifluoroacetic acid (Fig. 2 A).

Usually, a broad RP-HPLC peak is indicative of synthesis failure, but similar broad RP-HPLC elution peaks have been observed for other branched peptides, such as multiple antigenic peptides. They seem to be a consequence of the structural peculiarities of this type of analogue rather than an indication of poor synthetic quality (Veprek and Jezek, 1999).

The quality of the synthetic products was verified by matrix-assisted laser desorption ionization (MALDI) analysis (performed by Mass Consortium). Fig. 2 B shows results for the 15-residue–linked tandem gA. For the 23-residue–linked tandem gA, the spectrum depicts a series of Na^+ adduct peaks of a 5,580 molecular weight moiety, indicating that the peptide has the correct molecular weight.

Circular Dichroism Spectroscopy

The secondary structure of the bilayer-imbedded analogues was determined by circular dichroism spectroscopy at room temperature of the analogues incorporated into DMPC vesicles (Greathouse et al., 1999).

Electrophysiology

Planar bilayers were formed from *n*-decane solutions (2.5% wt/vol) of diphytanoylphosphatidylcholine (DPhPC) across a hole (~1.6-mm diameter) in a Teflon® partition that separates two aqueous solutions of unbuffered salt solution, usually 1.0 M CsCl, which was prepared fresh each day. Single-channel experiments were done at 25 ± 1°C using the bilayer punch technique with pipet tip diameters ~30 μm (Andersen, 1983a) and a Dagan 3900 patch clamp amplifier (Dagan Instruments) or an AxoPatch 1C patch clamp amplifier (Axon Instruments, Inc.). The gramicidins were added from ethanolic stock solutions to the electrolyte solution on either side of the bilayer. For most experiments, the gramicidin analogues were added to both sides of the bilayer. In some cases, two analogues were added asymmetrically—one analogue to one side and the other analogue to the other side. Single-channel current transitions usually were detected using a PC/AT-compatible computer using AxoBasic (Axon Instruments, Inc.) and using the algorithm described by (Andersen, 1983a); in some cases the current transitions were tabulated by hand. Single-channel current transition amplitude histograms and lifetime histograms were constructed as described previously (Andersen, 1983a; Sawyer et al., 1989). The lifetime histograms were transformed into survivor distributions, and the average channel lifetimes (τ) were determined by fitting a single exponential distribution: $N(t) = N(0) \cdot \exp\{-t/\tau\}$, where $N(t)$ denotes the number of channels with a lifetime longer than time t, to each histogram (Sawyer et al., 1989; Durkin et al., 1990).

RESULTS

General Characteristics of Gramicidins with Single-ended Tails and Tandem Gramicidins

Fig. 3 shows superimposed CD spectra obtained with standard gA, a gA analogue with a 7-residue single-

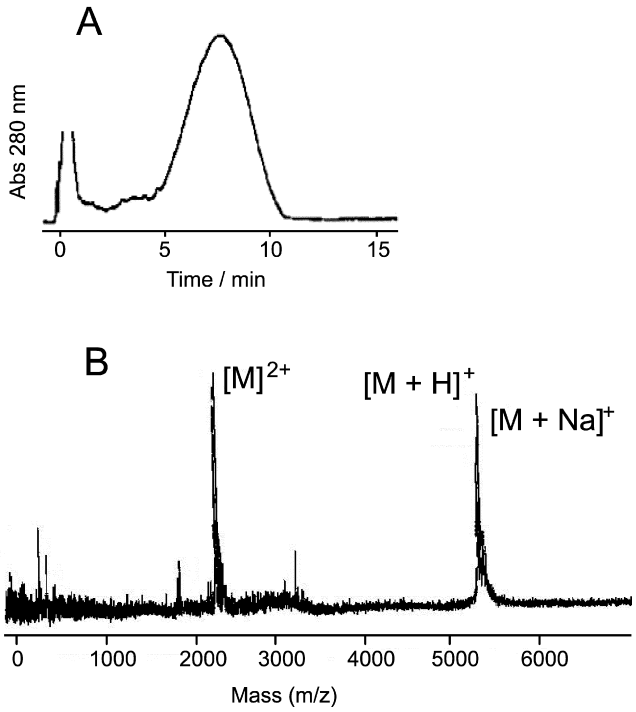

FIGURE 2. Characterization of the tandem gramicidin analogues. (A) RP-HPLC elution profile obtained with the 15-residue–linked tandem gramicidin gA. (B) MALDI spectra for the same compounds. The primary peak is an analogue-H^+ peak with a molecular weight of 5,210, equivalent to the predicted molecular weight of 5,209. Despite the rather broad elution profile the compound is of high purity as evident in the mass spectrum.

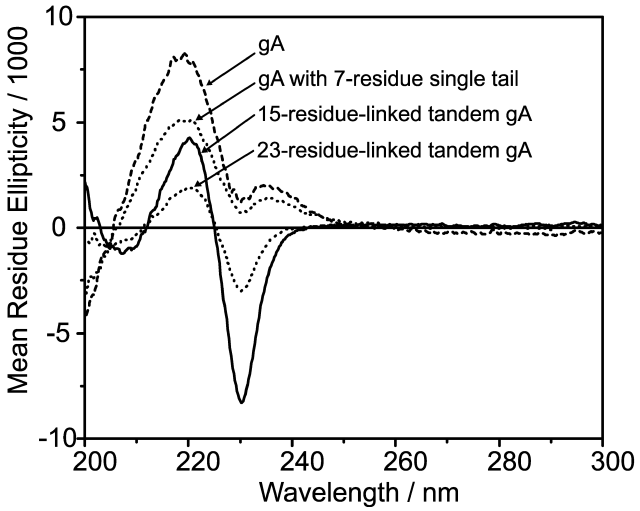

FIGURE 3. Circular dichroism spectra for the gramicidin analogues used in this study: gA, gA with the 7-residue eda tail, tandem gA with the 15-residue linker, and tandem gA with the 23-residue linker. DMPC vesicles.

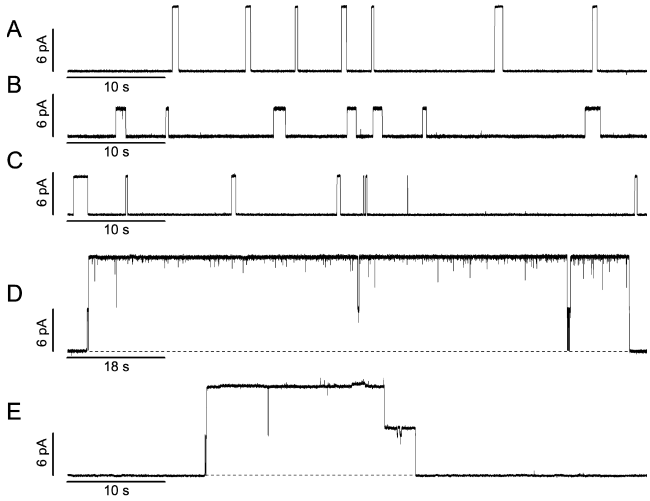

FIGURE 4. Single-channel current traces obtained with the gramicidin analogues used in this study (the channel type in D is shown at higher current and time resolution in Fig. 6). (A) gA. (B) gA with the 7-residue tail. (C) Tandem gA with the 15-residue linker. (D and E) Tandem gA with the 23-residue linker. 1.0 M CsCl, 200 mV, 200 Hz.

ended ethylene diamine (eda) tail, and the two tandem analogues in which two side-by-side subunits are covalently linked by either the shorter 15-residue or the longer 23-residue linker.

The CD spectra of gA and the analogue with the seven-residue single-ended eda tail are characteristic of the single-stranded, right-handed $\beta^{6.3}$-helical gA structure (the "channel" structure). The spectrum of the 15-residue-linked tandem gA represents a superimposition of single-stranded and double-stranded conformations. The spectrum of the 23-residue–linked tandem gA is similar to that for the 15-residue–linked analogue, although the negative peak at 232 nm is less pronounced, which is indicative of a smaller population of double-stranded conformations.

Fig. 4 shows single-channel current traces obtained with standard gA (Fig. 4 A), the gA analogue with a 7-residue single-ended eda tail (Fig. 4 B), as well as the two tandem gramicidin analogues, with the shorter 15-residue linker (Fig. 4 C) or the longer 23-residue linker (Fig. 4, D and E). (The results obtained with other analogues with single-ended tails were similar to those illustrated in Fig. 4 B; they are summarized in Table II.)

The analogue with single-ended tails, as well as the 15-residue–linked tandem gA analogue (Fig. 4, B and C), form rather "standard" channels, with properties that generally resemble those of the standard gramicidin channels formed by the "wild-type" gA (Fig. 4 A): the individual conductance steps are well resolved, with occasional poorly resolved downward transitions (e.g., in Fig. 4 B). Of particular importance, the channels formed by gA subunits linked by the shorter 15-residue-linker are very similar to the channels formed by gA subunits with single-ended tails, which suggests that this linker is too short to allow for the formation of double-barreled channels.

Characteristics of Double-Barreled gA Channels

A quite different result is observed in the case of gA subunits that are coupled by the longer 23-residue linker (Fig. 4, D and E). In this case, the channels' lifetimes are much longer than was the case for any of the other analogues, and at the resolution of the figure, the current transition amplitudes in Fig. 4 D appear to be almost twofold higher than was the case for the gA subunits with single-ended tail segments; but, there is evidence for transitions to intermediate current levels when the channels appear and disappear, as well as in the middle of the trace. The current transition amplitude and lifetime histograms for the channels formed by these four gramicidins are shown in Fig. 5; the results for all analogues, as well as gA, are summarized in Table II.

Standard gA (Figs. 4 A and 5 A), the analogue with a 7-residue single-ended eda tail (Figs. 4 B and 5 B), and the 15-residue–linked tandem gA analogue (Figs. 4 C and 5C) form channels that differ little—except that the single-channel current transitions observed with gA are almost twice those observed with the analogues; the channel lifetimes differ twofold, but with no obvious systematic pattern. The current through the channels formed by the analogue with the 7-residue single-ended eda tail is less than that through the other analogues, which presumably is due to the net positive charge at the end of the linker; but there is no evidence

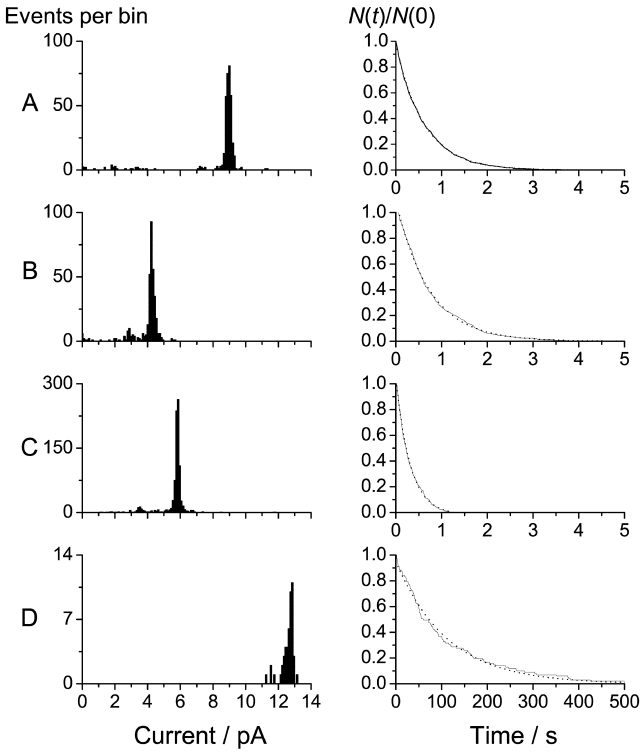

FIGURE 5. Current transition amplitude histograms (left) and lifetime distributions (right) for channels formed by: A, gA; B, gA with the 7-residue tail; C, 15-residue–linked tandem gA; and D, 23-residue–linked tandem gA. The current transition histograms were determined at 200 mV. The lifetime distributions for gA, gA with the 7-residue tail, and the 15-residue-linked tandem were also determined at 200 mV; the lifetime distributions for the 23-residue-linked tandem gA is based on results obtained at 100 and 200 mV. 200 Hz.

TABLE II

Conductances and Lifetimes for Channels Formed by gA, gA Analogues with Single-ended Tails, and Tandem gA Channels

Analogue	Conductance/pS (mean ± SD)	Lifetime/ms (mean)
gA	50.4 ± 1.0	720
gA with 7-residue eda tail	21.2 ± 1.2	670
gA with 7-residue ea tail	29.5 ± 0.9	610
gA with 13-residue ea tail	29.2 ± 0.8	300
15-residue–linked tandem gA	33.4 ± 2.3	530
23-residue–linked tandem gA	63.5 ± 1.7[1]	110,000

1.0 M CsCl, 200 mV, except that the lifetime for the 23-residue–linked tandem gA channels is based on results at 100 and 200 mV. The brief flickers to the intermediate current levels were disregarded when measuring the lifetime of the channels formed by the 23-residue-linked tandem gA.

[1]The current through the long-lived (double-barreled) channels.

for discrete transitions between two conductance levels, as would be expected if the positive charge were localized in a few defined places (Woolley et al., 1997). By analogy, the linkers in the tandem gramicidins are likely to be (more or less) freely mobile.

The 23-residue–linked tandem analogue (Figs. 4 D and 5 D), however, forms channels that differ qualitatively from the channels formed by the other analogues. The full current transitions are about twofold higher than those observed for the channels formed by the analogue with the single-ended tail and the 15-residue–linked tandem analogue, there are transitions to intermediate current levels, and the lifetimes are ~200-fold longer. As can be seen in Fig. 4, the 23-residue–linked tandem gA forms two, qualitatively rather different, channel types. The predominant type is that shown in Fig. 4 D. Infrequently (~5% of the observed events), the channels exhibit the behavior shown in Fig. 4 E, in which the transition pattern is distinctly different from that in Fig. 4 D—as the intermediate conducting state, which is barely visible in Fig. 4 D, now has a lifetime that may be many seconds. Given the rarity of these events, we did not investigate them in any detail, and the quantitative analysis that follows is based only on channel events of the type shown in Fig. 4 D.

The differences between the channels formed by the 23-residue–linked tandem analogue and the channels formed by gA or the analogues with a single-ended tail or the 15-residue linker become more pronounced when the channels formed by the 23-residue–linked tandem analogue are examined at higher time resolution (Fig. 6). The larger current transitions in Fig. 4 D now are seen to be composite events, in which there is an initial bursting channel activity that is followed by a two-step increase of the current to a new level, which is maintained for up to several minutes.

In ~25% of the appearances, the initial bursting channel activity occurs in isolation, i.e., with no subsequent two-step transition to the higher current level (an example of such a channel is shown at the bottom of Fig. 6). The more common pattern, however, is a transition from the bursting channel activity to a second, higher current level (top two rows of traces in Fig. 6). The two rows show examples where the two-step channel appearances occur in the presence or absence of preceding bursting activity. (In the middle set of traces, channel disappearance is followed by a bursting event.) Once the higher current level is reached, the current is remarkably stable, with only occasional transitions to a flickery state (see also Fig. 4 D). When the current activity ceases, the transition to the baseline is usually composite with a brief sojourn at an intermediate level, which may or may not exhibit bursting activity similar to that observed before the two-step channel formation. For either composite transition, each of the individual current transition amplitudes is comparable to those of the channels formed by analogues with sin-

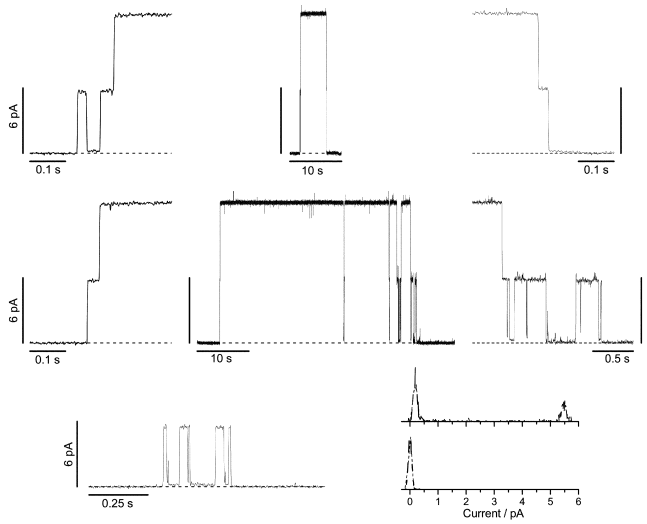

FIGURE 6. Bursting channel activity and formation and disappearance of channels formed by the 23-residue–linked tandem gA. The top two rows of traces show two different examples of double-barreled channel appearance/disappearance patterns in which the transition to the fully conducting level proceeds through an intermediate conductance level. In each row, the traces to the right and left of the complete channel show the appearance/disappearance transitions at higher time resolution. To better visualize the various conductance states, the interrupted lines in each trace are drawn through the baseline, when no channel is conducting. (Top row) Channel formation is preceded by bursting channel activity with no bursting activity when the channel disappears. (Middle row) There is no bursting channel activity preceding channel formation, but there is bursting activity after the channel disappearance—as well as an isolated bursting event that follows closely after the disappearance of the double-barreled channel. (Bottom three panels) Isolated bursting channel activity. The histograms to the right show that the burst reflects transition within a bilayer-spanning dimer; the two current level histograms at the right were recorded during the bursting channel activity (top histogram) and just before (bottom histogram). 200 mV, 200 Hz.

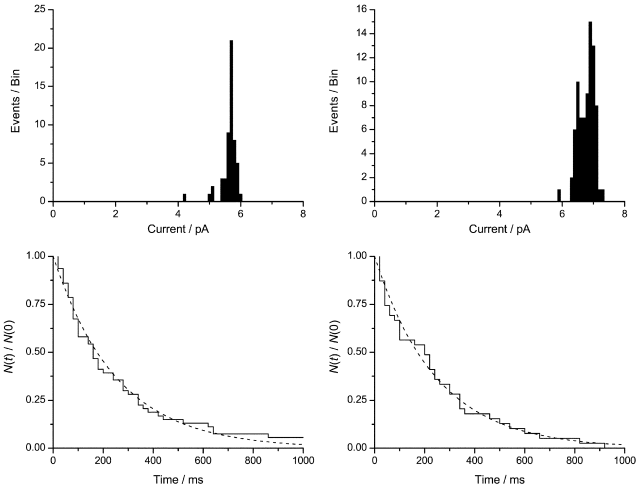

FIGURE 7. Current transition amplitude and lifetime histograms for the appearance and disappearance of the double-barreled channels formed by the 23-residue–linked tandem gA. (Top) Current transition amplitude histograms. (Left) Histogram for the initial transition from the baseline to the intermediary current level. (Right) Histogram for the final transition from the double-barreled to intermediary current level. (Bottom) Lifetime distributions. (Left) The interval distribution for the durations of bursting transition when the double-barreled channel appears. (Right) The interval distribution for the durations of bursting transition when the double-barreled channel disappears. The results, as well as those for the bursting and flickery channels are summarized in Table III. 1.0 M CsCl, 200 mV, 200 Hz.

gle-ended tails. Given how infrequently these long-lived composite events appear/disappear (the experiments were done at appearance rates that were $<0.01\ s^{-1}$, often much less), we conclude that these events represent the formation and disappearance of double-barreled channels.

Closer inspection of the current traces in Fig. 6 shows that the bursting channel activity represents transitions within a bilayer-spanning pore because the lower of the two current levels within the burst is above the baseline current—where no channel is conducting. This is quantified in detail for the case of bursting channels in the current level histograms at the bottom of Fig. 6. Similar results were also obtained for the channel appearances and disappearances; the results are summarized in Table III. Due to difficulties in identifying a 0.2-pA transition from the baseline to (or from) the low-conductance current level in the bursting events, it is not clear if the channel appearances always are from the baseline to the 6-pA intermediate current level, and vice versa for the disappearances. To minimize ambiguities, we identify the channel appearances and disappearances to begin (or terminate) with the first (or last) transition to (or from) the 6-pA current level.

The composite current transitions during channel appearances/disappearances are not of equal height. This is evident in the current traces in Figs. 4 D and 6, and it is shown in detail in Fig. 7, which shows current transition amplitude and lifetime histograms for the channel appearances and disappearances. The results, as well as those for the other transitions, are summarized in Table III.

When the double-barreled channel appears, the second transition is ~15% higher than the first; similarly, when the double-barreled channel disappears, the first transition (from the full to the intermediate level) is ~15% higher than the second (to the baseline). There are occasional transitions from the double-barreled channel to an intermediate, flickery event (e.g., Figs. 4 D and 6), which is indistinguishable from the events that precede or follow the double-barreled channels (Fig. 6 and Table III). As is the case for bursting events that initiate or terminate a double-barreled event, the low-conductance state within the burst is above the

TABLE III

Summary of Current Transitions and Lifetimes for the Brief Transitions Observed with the 23-residue–linked Tandem gA

A. Current transitions

Transition	Bursts (mean ± SD)	Appearances (mean ± SD)	Flickers (mean ± SD)	Disappearances (mean ± SD)
	Δi/pA	*Δi/pA*	*Δi/pA*	*Δi/pA*
Baseline to substate	0.24 ± 0.7	0.23 ± 0.06		0.27 ± 0.05
Substate to intermediate	5.40 ± 0.23	5.53 ± 0.09	5.46 ± 0.15	5.52 ± 0.08
Baseline to intermediate	5.63 ± 0.38	5.70 ± 0.17		5.76 ± 0.15
Intermediate to full		6.90 ± 0.28	6.79 ± 0.22	6.90 ± 0.26

B. Lifetimes

Bursts (mean)	Appearances (mean)	Flickers (mean)	Disappearances (mean)
τ/ms	*τ/ms*	*τ/ms*	*τ/ms*
690	250	260	250

A, 1.0 M CsCl, 200 mV. B, 1 M CsCl, results obtained at 100 and 200 mV. Estimates for τ are based on single exponential fits to the lifetime distributions, except for the bursting channels where a simple average was used.

baseline current, as can be seen by comparing the transition amplitudes for the low-to-intermediate current transition during appearances/disappearances with those for the flickery transitions from the double-barreled current level (Table III).

Given the two-state behavior of the bursting channels, as well as the appearance and disappearance events of the double-barreled, one would expect the lifetime distributions to deviate from single exponential distributions. Somewhat surprisingly, the lifetimes of the appearance and disappearance steps are quite well fit by single exponential distributions (Fig. 7), and so is the lifetime distribution for the flickery events (unpublished data). The bursting events, however, had a lifetime distribution that was not well fit by either a single- or a double-exponential distribution, and we estimate the average lifetime as a simple average of the observed lifetimes. Another surprise is that the average lifetime of the bursting channels is twofold longer than those for the three types of brief channel events, which are indistinguishable. We discuss the implications of this finding in the DISCUSSION. (Because of the very long lifetimes of the double-barreled channels, the experiments had to be done at very low channel appearance rates, and the total number of observed channel events was insufficient for a more detailed analysis of the lifetime distributions.)

Though we did not examine the channels with the appearance pattern in Fig. 4 E in any detail, we noted that the intermediate current level invariably was higher than was the case for the bursting events or the intermediate current level during "normal" appearances/disappearances—and that there were transitions between this higher level and a current level similar to that usually observed (compare Fig. 4 E). The molecular basis for these transitions remains unclear.

Heterodimer Experiments

What is the basis for the different current transition amplitudes in the double-barreled channels? The CD spectra (Fig. 3) show that the tandem analogues form both $\beta^{6.3}$-helical and non-$\beta^{6.3}$-helical structures; but, the rather modest differences in single-channel current and lifetime between the channels formed by gA and the analogues with a single-ended tail suggest that the structure of the bilayer-spanning channel is not altered by attaching an extension at Trp^{15}. Nevertheless, could there be an intrinsic asymmetry between the channel subunit that is linked to the α NH group, as opposed to the ε NH group? These questions were addressed in heterodimer formation experiments, which constitute a sensitive test for whether a given sequence modification alters the channel structure (Durkin et al., 1990). Basically, if a gramicidin analogue forms only one type of channel, and if heterodimeric channels can form between the analogue and a reference gramicidin of known structure (e.g., gA), we may conclude that the analogue can fold such as to adapt to the structure of the reference subunit. (Ideally, one should examine the relative distribution between the two homodimers and the corresponding heterodimers, which in the case of structural invariance is described by the binomial distribution [Durkin et al., 1990; Durkin et al., 1993]. In practice, the long lifetimes of the 23-residue–linked tandem gA channels preclude this measurement.)

Therefore, we did heterodimer experiments with gA as the reference subunit opposite an analogue with a

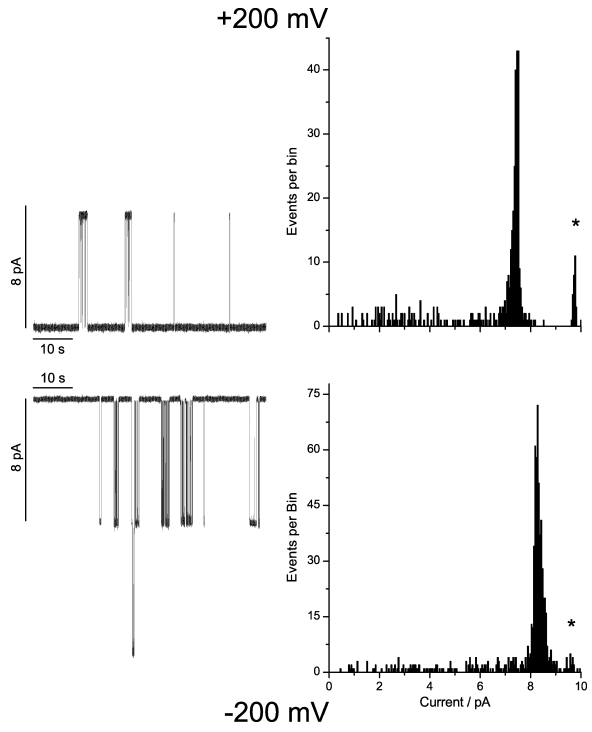

FIGURE 8. Heterodimer experiment with the 23-residue–linked tandem gA, and gA. The two gramicidins were added to opposite sides of a bilayer, and the gA-containing solution is the electrical reference. Left, current traces; right, current transition amplitude histograms. Top, results at +200 mV; bottom, results at −200 mV. The smaller peak, marked by an asterisk, denotes homodimeric gA channels due to an avoidable, if slow, "leak" of gA across the bilayer. The results are summarized in Table IV. 200 Hz.

7-residue single-ended eda tail, as well as the 15-residue–linked or 23-residue–linked tandem analogues. In each case, we observed heterodimeric channels—formed between the reference gA and the analogue. The experiments were done using asymmetric addition of the two analogues, with the reference gA being present at only one side of the bilayer and the analogue on the other side, such that there is only a single orientation of the heterodimeric channels. Fig. 8 shows the current traces and current transition amplitude histograms obtained with gA and the 23-residue–linked tandem analogue at ±200 mV; the results for the other experiments are summarized in Table IV.

Comparing the histograms in Fig. 8 with those in Fig. 5, it is apparent that a new channel type, the heterodimer, forms when the two different gramicidins are added together. Importantly, only a single predominant channel type is seen at each polarity. Therefore, we conclude that the intrinsic permeability properties of the channels formed by the two subunits in the 23-residue–linked tandem gA are indistinguishable, which means that the different current transition amplitudes

TABLE IV

Conductances of Heterodimeric Channels Formed between gA and the Two Tandem Gramicidin Analogues as well as the Analogue with a 7-residue Single-ended Tail

Test analogue	−200 mV	200 mV
	g/pS	*g/pS*
gA with 7-residue eda tail	41.7 ± 1.3	26.3 ± 1.2
15-residue tandem gA	43.7 ± 3.5	38.8 ± 2.6
23-residue tandem gA	41.4 ± 1.5	37.2 ± 0.9

1.0 M CsCl, 200 mV. Potentials are relative to the gA-containing solution.

for the first and second transition in Figs. 4 and 6 arise because of interactions between the two barrels.

Moreover, the current transition amplitudes at the two polarities differ: for all the heterodimers, the transitions are larger at negative potentials, when the net ion movement is from the gA subunit to the analogue subunit with a single-ended tail or a linker (Fig. 8 and Table III). The linker residues thus appear to constrain ion entry into the pore. Examination of the −200 mV current trace in Fig, 8 shows that the channels again occur in bursts, in which the current switches between a high-conductance state ($i \approx 8$ pA) and a low-conductance state ($i \approx 0.2$ pA). We did not pursue this further,[1] but concluded that the two barrels of the tandem gramicidins have intrinsic permeability properties that are indistinguishable.

We also did asymmetric heterodimer experiments with the 15- and the 23-residue lined tandem gramicidin analogues, where we (again) added the two analogues to opposite of the bilayers. In this case, there was no asymmetry between the currents at ±200 mV, both of which were ∼6.2 pA, again indicating that the linked subunits have indistinguishable permeability characteristics.

Basis for the Unequal Current Transitions

What could be the mechanistic basis for the different current transition amplitudes from the baseline to the intermediate current level (corresponding to just one conducting channel), as compared with the transition from the intermediate to the composite current level (corresponding to two conducting channels)? The difference is unlikely to result from structural differences between the two channels, as we observe only a single population of current transition amplitudes for the heterodimers formed between gA and the 23-residue–

[1]The similar low-conductance current levels in the bursting and appearance/disappearance events observed with symmetrical channels formed by the 23-residue–linked tandem gA (Fig. 6 and Table III) may indicate that the transitions between the intermediate- and the low-conductance states arise, at least in part, from some conformational changes that influence ion dissociation from the channel.

linked analogue (Fig. 7). It also is unlikely that it always would be the same variant of two different channel types that formed the first channel in the double-barreled construct.

Accepting that the unequal current steps do not result from chemically dissimilar "barrels," we need to consider two possible explanations for the observation. First, if the linker partially occluded the first barrel of a pair, this steric hindrance could be removed (in part) when the second channel opened. Second, and mechanistically more interesting, the energetic barrier for ion movement through each of the pores could be lower for a pair of channels, as compared with an isolated channel. It is well established that the energy barrier for ion movement through a channel is a function of the dielectric constant of the surrounding bilayer (Parsegian, 1969; Levitt, 1978; Jordan, 1986), and a bilayer-spanning channel constitutes a more polar environment than the bilayer hydrophobic core. So, if the two barrels were sufficiently close together the electrostatic barrier for moving an ion through each pore would be reduced because some of the acyl chains surrounding each channel have been replaced by the other bilayer-spanning barrel.

To distinguish between these two possibilities, we did experiments using 0.1 M CsCl, where aqueous diffusion limitations would be more pronounced (compare Andersen, 1983a), and 1.0 M NaCl, in which the currents (in gA channels) are similar to that in 0.1 M CsCl, but where the barrier for ion movement through the pore would be relatively more important than the entrance barrier. The basic pattern of composite channel appearances/disappearances is seen also under each of these ionic conditions. The results on current transition amplitudes are summarized in Table V, which also summarizes the results obtained in 1.0 M CsCl.

Relative to gA, the Cs^+ permeability is reduced more than for Na^+ permeability, which suggests that the linker indeed constrains diffusional ion access to the pore entrance. The main result, however, is that the relative difference between the two current transition amplitudes is less in 0.1 M CsCl, where diffusion limitations will be more pronounced. Thus, these results are consistent with a lower barrier for ion movement through each barrel of the side-by-side pair, suggesting that the two barrels indeed are in close apposition.

TABLE V

Permeability Properties of Channels Formed by the 23-residue Tandem gA

Salt	gA channels	23-residue–linked tandem gA channels		
	i/pA (*mean ± SD*)	$\Delta i_1/pA$ (*mean ± SD*)	$\Delta i_2/pA$ (*mean ± SD*)	$\Delta i_2/\Delta i_1$ (*mean ± SEM*)
		100 mV		
0.1 M CsCl	1.57 ± 0.05	1.03 ± 0.05	1.16 ± 0.08	1.12 ± 0.01
1.0 M CsCl	4.92 ± 0.30	3.57 ± 0.16	4.21 ± 0.15	1.17 ± 0.01
1.0 M NaCl	1.31 ± 0.06	1.12 ± 0.04	1.30 ± 0.08	1.17 ± 0.02
		200 mV		
0.1 M CsCl	2.40 ± 0.24	1.43 ± 0.09	1.54 ± 0.11	1.06 ± 0.01
1.0 M CsCl	10.04 ± 0.20	5.69 ± 0.27	6.83 ± 0.25	1.21 ± 0.01
1.0 M NaCl	3.02 ±0.15	2.11 ± 0.11	2.42 ± 0.08	1.14 ± 0.01

The results for Δi_1 and Δi_2 are based on composite appearance and disappearance transitions, as well as flickery and intermediate events. The results for $\Delta i_2/\Delta i_1$ are based on the ratios of the current transitions in individual composite appearance and disappearance events.

DISCUSSION

When two gramicidins are covalently linked at their carboxy termini, with a sufficiently long linker, the resulting analogues form double-barreled channels, with coordinated formation (and dissociation) of the two barrels. Once both barrels form, the resulting channels have lifetimes that are more than two orders of magnitude longer than the lifetime of single-barreled gramicidin channels having similar sequences (in their bilayer-spanning domains). The long lifetimes and "stable" single-channel currents show that two bilayer-spanning barrels indeed can be coupled at the functional level. Given that the gramicidin channels are imbedded fully in the bilayer, the coupling most likely is due to bilayer-mediated interactions.

We first discuss the evidence that the long-lived events indeed are double-barreled channels. Next, we discuss the significance of the different amplitudes of the current transition from the baseline to the intermediate current level, as compared with the transition from the intermediate to the high-conductance level, and conclude that the two barrels are in very close, side-by-side contact. Then, we address the mechanistic basis for the stability of the double-barreled channels, and conclude that the stability results because the elastic force imposed by the bilayer deformation acts on both barrels, such that the force/barrel is less than for the standard, single-barreled gA channel. Finally, we discuss some implications of these results.

Evidence for Double-barreled Channels

In principle, the composite channel events could form either between two 23-residue–linked analogues (one on each side of the bilayer) or between three such analogues (one on one side and two on the other side of the bilayer). Two lines of evidence indicate that the composite channels predominantly are double-barreled channels—formed between two 23-residue–linked analogues. First, we observe no such composite events with the 15-residue–linked analogues—at least not under conditions that allow for single-channel experiments. Second, the experiments were done under conditions where the bursting and composite channel events occur at a rate $<10^{-2}\ s^{-1}$ (compare Figs. 4, D

and E, and 7), whereas the transition from the first to the second current level occurs at a rate >1 s^{-1} (Fig. 7 and Table III). Thus, only a small fraction of the composite events will form as daisy chains between three of the linked analogues. We conclude that the composite events indeed are double-barreled channels. Rokitskaya et al. (2003) similarly conclude that gA channels that are coupled using a biotin-streptavidin–induced cross-linking also are double-barreled channels.

Origin of the Unequal Current Transitions

Given the single population of current transition amplitudes in the heterodimer experiments with gA and both the 15- and 23-residue–linked analogues (Fig. 8 and Table III), the pattern of current transitions in the composite events becomes striking. Not only are the two current transition amplitudes distinct; but, the first transition is (almost) invariably the smaller of the two. This pattern differs qualitatively from the one that usually is expected to occur, namely that channel clustering decreases the current amplitude due to local depletion of permeant ions (e.g., Neumcke and Stämpfli, 1983). (The present situation is similar to that observed for alamethicin, which forms multistate channels where the conductance of every next step is higher than that of the preceding step [Gordon and Haydon, 1972; Eisenberg et al., 1973], but with little change in pore radius—as deduced from polymer partitioning [Bezrukov and Vodyanoy, 1993].) The different current transition amplitudes in the composite events somehow must reflect local interactions between the two barrels in the double-barreled channels, which could occur for two reasons. First, the dynamics of the linker close to the pore entrance could be constrained in the double-barreled channels so as to reduce the restrictions on ion access to the pore. Second, electrostatic interactions between the two pores could reduce the electrostatic barrier for ion movement through the pore.

Though the linker most likely reduces the rate constant for (diffusional) ion access to the pore, the results in Table V exclude the possibility that the difference between the two current transition amplitudes results from relative changes in access. Importantly, compared with 1.0 M CsCl or NaCl, the difference between the two current transition amplitudes is decreased in 0.1 M CsCl, where diffusion-controlled ion access is more important (Andersen, 1983b)—and more so at 200 mV where ion access will be most important. We also note that Rokitskaya et al. (2003), using a completely different linker strategy, observe a similar difference between the first and second transition amplitude as we do, which would tend to exclude a specific action of the linker. Moreover, even in the case of channels formed by the analogue with the 7-residue single-ended eda tail (Fig. 4 A, Table II), there is no evidence for fast transitions between two current levels, similar to those observed by Woolley et al. (1997) using a shorter linker. That is, the positive charge at the end of the linker seems to move rather freely.

In the next section we conclude that the linker seems to be sufficiently flexible to impose little restriction on the formation of the second barrel, which also would tend to exclude local effects on ion access. We therefore conclude that the pattern of current transition amplitudes results from changes in the barrier for ion movement through the pore itself. It is difficult to envisage how this coupling could arise unless the two barrels were in quite close apposition. If the two barrels, for example, were separated by only one phospholipid molecule, the effective dielectric constant of their surroundings would be increased over that of the bilayer core, which will lower the energy barrier for ion movement through the pore (Parsegian, 1969; Levitt, 1978; Jordan, 1986). In addition to this effect, the different current transitions also could result from changes in the average orientation of one or more of the tryptophan residues at the channel entrance, which again would alter the barrier for ion movement through the pore (Becker et al., 1991; Andersen et al., 1998).

Formation and Stability of Double-barreled Channels

Standard gA channels usually form in a single step—although composite transitions also are observed (Busath and Szabo, 1981; Sigworth and Shenkel, 1988; Mobashery et al., 1997), where the intermediate current levels usually are of brief duration. The pattern of channel appearances observed with the 23-residue–linked tandem analogue is quite different from that usually observed with gA, as the first pore does not form in a single, "clean" step to a well-defined current level, but rather presents itself as a series of rapid transitions between two current levels. This bursting channel behavior usually lasts <1 s, and it ceases when the second pore forms (Fig. 5). Similar behavior was observed by Rokitskaya et al. (2003), who used a biotin/streptavidin strategy to form double-barreled channels, although in their case the bursting behavior could last many seconds. Somewhat surprisingly, we did not observe double-barreled heterodimeric channels between the 15- and the 23-residue–linked tandem gAs. This most likely reflects that subunit folding is compromised when the linker is too short, as the 15-residue–linked tandem gA has a much more negative ellipticity at 230 nM, which is indicative of a larger fraction of non-$\beta^{6.3}$-helical subunits, than the other analogues (Fig. 3). It also could indicate that a critical linker length is necessary in order for double-barreled channels to form, e.g., because the two monomeric subunits in a single-barreled channel formed by the 15-residue–linked tandem gA are held at positions that do not allow for dimerization.

The question remains, why does the 23-residue–linked tandem analogue form bursting channels? Mobashery et al. (1997) showed that the kinetics of gA channel formation changes qualitatively, with the appearance of bursting events, when the difference between bilayer thickness and channel length exceeds some critical value. These bursting events occur at gramicidin concentrations that are ~100-fold higher than the ones normally used (in DPhPC bilayers). The presence of monomers in relatively close proximity may alter the kinetics of dimerization; we do not understand why.

Though their kinetics are complex, the average lifetime of the (single-barreled) bursting channels formed between two 23-residue–linked tandem analogues is twofold larger than the lifetimes for the double-barreled appearance/disappearance transitions. This was unexpected because the initial formation of a single-bilayer-spanning channel between two 23-residue–linked tandem gAs will terminate either because the conducting dimer dissociates (with rate constant k_{-1}) or because the second bilayer-spanning channel forms (with rate constant k_{+2}). (In the discussion that follows we will not consider the two-state nature of the single-barreled, bursting channels.) The same two rate constants would describe the kinetics of channel appearances, flickers from the double-barreled state, and disappearances. One thus would expect that the lifetimes of the bursting channels, the appearance transitions, the flickery transitions, and the disappearance transitions should have identical lifetimes ($\tau_1 = (k_{-1} + k_{+2})^{-1}$). The results in Table III show that to be the case for the latter three types of transitions, but not for the bursting channels. The parsimonious explanation for this "discrepancy" is that some tandem gramicidins may have one subunit that is not folded as a $\beta^{6.3}$-helix, as the CD spectra (Fig. 3) show that a significant fraction of not only the 15- but also the 23-residue–linked tandem gAs fold into non-$\beta^{6.3}$-helical structures. If, for example, only 50% of the gA subunit in the 23-residue–linked tandem gA were $\beta^{6.3}$-helices, it would account for the observed differences between the lifetimes for the different types of transitions. (It also could account for the kinetic complexity of the lifetime distribution for the bursting channels.) The relative partitioning between subunit dissociation and double-barreled channel formation is k_{+2}/k_{-1}, or ~3, which means that $k_{+2} = \tau_{+1}^{-1}/(1 + k_{+1}/k_{+2}) \approx 3\ s^{-1}$.

k_{+2} is the pseudo-first order rate constant for the formation of the second barrel in the double-barreled channel. To a first approximation, for a flexible linker, $k_{+2} = k_{+1} \cdot [gA]$, where k_{+1} is the rate constant for gA dimerization, and [gA] is the (local) concentration of gA monomers around the first barrel. Taking the extended length of the linker, ~14 nm, as a measure of how far the single, uncoupled subunit can move, [gA] $\approx 10^{-3}$ molecules/nm^2. In DPhPC/*n*-decane bilayers $k_{+1} \approx 10^4$ nm^2/(s·molecule) (Rokitskaya et al., 1996), so assuming no interactions between the subunits, k_{+2} is expected to be ~10 s^{-1}. This estimate is in good agreement with the experimental estimate of 3 s^{-1} (Table III); we conclude that the linker is unlikely to impose significant stress on the subunit interactions.

For single-barreled gramicidin channels, the channel formation/disappearances are described by Scheme I (cf. Bamberg and Läuger, 1973; Veatch et al., 1975),

$$2\ M \rightleftarrows D,$$

SCHEME I

where M and D denote the mole-fractions of nonconducting monomers and conducting dimers in the bilayer. The standard free energy of dimerization, ΔG^0_{tot}, is given by

$$\frac{[D]}{[M]^2} = \exp\{-\Delta G^0_{tot}/k_B T\} = \exp\{-(\Delta G^0_{prot} + \Delta G^0_{def})/k_B T\}, \quad (1)$$

where k_B is Boltzmann's constant, T the temperature in Kelvin, and ΔG^0_{prot} and ΔG^0_{def} the intrinsic and bilayer-dependent contributions to ΔG^0_{tot} (compare Andersen et al., 1999). ΔG^0_{prot} is determined by, among other factors, the hydrogen bonds that stabilize the bilayer-spanning dimers. ΔG^0_{def} is determined by the channel-bilayer interactions, in particular the bilayer deformation associated with forming the channels, as the average thickness (d_0) of the unperturbed bilayer (~4.3 nm in the case of DPhPC/*n*-decane bilayers based on a bilayer specific capacitance of 4.3 nF/mm^2; cf. Redwood et al., 1971) is larger than the channel's hydrophobic length (l, ~2.3 nm; Elliott et al., 1983). The channel–bilayer interactions are well described using an elastic bilayer model (Nielsen et al., 1998; Lundbæk and Andersen, 1999):

$$\Delta G^0_{def} = H_B \cdot (d_0 - l)^2, \quad (2)$$

where H_B is a phenomenological spring constant, which is ~8 kJ/(mole·nm^2) for monoglyceride/*n*-decane bilayers (Lundbæk and Andersen, 1999) and ~20 kJ/(mole·nm^2) for DPhPC/*n*-decane bilayers (unpublished data). Thus, ΔG^0_{def} will be a significant, ~80 kJ/mole, destabilizing contribution to ΔG^0_{tot}.

For double-barreled gramicidin channels, the channel formation/disappearances are described by Scheme II,

$$2\ M\text{-}M \rightleftarrows M\text{-}D\text{-}M \rightleftarrows D\text{-}D,$$

SCHEME II

where M-M denotes the linked monomeric subunits, M-D-M the single-barreled channel with two linked sub-

units, and D-D the linked double-barreled channel. In this case, the standard free energies of dimerization for the single-barreled (M-D-M) and double-barreled (D-D) channels, $\Delta G^{0,1}_{tot}$ and $\Delta G^{0,2}_{tot}$, are given by,

$$\frac{[\text{M-D-M}]}{[\text{M-M}]^2} = \exp\{-\Delta G^{0,1}_{tot}/k_BT\} = \exp\{-(\Delta G^{0,1}_{prot} + \Delta G^{0,1}_{def})/k_BT\}, \quad (3)$$

and

$$\frac{[\text{D-D}]}{[\text{M-M}]^2} = \exp\{-\Delta G^{0,2}_{tot}/k_BT\} = \exp\{-(\Delta G^{0,2}_{prot} + \Delta G^{0,2}_{def})/k_BT\}, \quad (4)$$

To a first approximation the formation of a single-barreled channel should not be significantly affected by the presence of the other subunit in the tandem gramicidin, in which case $\Delta G^{0,1}_{tot} \approx \Delta G^{0}_{tot}$, $\Delta G^{0,1}_{prot} \approx \Delta G^{0}_{prot}$, and $\Delta G^{0,1}_{def} \approx \Delta G^{0}_{def}$.

To evaluate the relative stabilization of the double-barreled channels we note that gA channels obey Poissonian statistics (Hladky and Haydon, 1972; Andersen, 1978), such that the probability of observing one and two conducting channels ($W(1)$ and $W(2)$, respectively) is given by $\lambda \cdot \exp\{-\lambda\}$ and $(\lambda^2/2) \cdot \exp\{-\lambda\}$, where λ is the average number of conducting channels: $\lambda = f \cdot \tau$, where f is the channel appearance rate and τ is the channel lifetime. That is, if there were no interactions among the bilayer-spanning channels, the relative distribution between two-channel and one-channel events, $W(2)/W(1)$, would be given by $\lambda/2$. The stabilization of the double-barreled channels thus can be described as the ratio between the observed and expected distribution between double-barreled [D-D] and single-barreled [M-D-M] channels. The observed distribution is [D-D]/[M-D-M] and, according to Poisson statistics, the expected distribution is [M-D-M]/2. The relative stabilization thus becomes

$$\frac{\frac{[\text{D-D}]}{[\text{M-D-M}]}}{\frac{[\text{M-D-M}]}{2}} = 2 \cdot \frac{[\text{D-D}]}{[\text{M-M}]^2} = \exp\left(\frac{-\Delta\Delta G^0}{k_BT}\right), \quad (5)$$

such that $\Delta\Delta G^0 = 0$ when the distribution between single- and double-barreled channels is described by the Poisson distribution. $\Delta\Delta G^0$ then can be expressed as

$$\Delta\Delta G^0 - k_BT \cdot \ln 2 = \Delta G^{0,2}_{tot} - 2 \cdot \Delta G^{0,1}_{tot} = (\Delta G^{0,2}_{prot} - 2 \cdot \Delta G^{0,1}_{prot}) + (\Delta G^{0,2}_{def} - 2 \cdot \Delta G^{0,1}_{def}). \quad (6)$$

In Eqs. 3–6, the ΔG_{prot} contributions to ΔG_{tot} reflect both the hydrogen bond organization at the subunit interfaces, which should be invariant, and the increased monomer concentration around the single-barreled M-D-M channels (Jencks, 1981; Creighton, 1993), which means that $\Delta G^{0,2}_{prot} \neq 2 \cdot \Delta G^{0,1}_{prot}$. If the linker is flexible, such that it does not impede monomer association: $\Delta G^{0,2}_{prot} < 2 \cdot \Delta G^{0,1}_{prot}$; if the linker impedes monomer association: $\Delta G^{0,2}_{prot} > 2 \cdot \Delta G^{0,1}_{prot}$, and the local concentration could, in principle, be zero if the linkers forced the monomers apart to preclude the formation of the second barrel. Similarly, the ΔG_{def} contributions will not be additive because ΔG_{def} varies as a function of channel radius (circumference) (Nielsen et al., 1998) such that $\Delta G^{0,2}_{def} < \Delta G^{0,1}_{def}$.

To evaluate $\Delta\Delta G^0$, we note that the experiments were done at a channel appearance rate of 0.01 s^{-1} (or less), that the average lifetime of the single-barreled events is ~0.25 s, that ~75% of the single-barreled channels convert into double-barreled channels, and that the lifetime of the double-barreled channels is ~100 s. That is $2 \cdot [\text{D-D}]/[\text{M-D-M}]^2 \approx 2 \cdot 0.75 \cdot 0.01 \cdot 100/(0.01 \cdot 0.25)^2 \approx 2 \cdot 10^5$, or $= \Delta\Delta G^0 \approx 30$ kJ/mole. For comparison, we note that the making or breaking of one hydrogen bond corresponds to 10–15 kJ/mole (Schulz and Schirmer, 1979; Fersht, 1987).

Some of the stabilization results from the increased local monomer concentration that is associated with formation of the first barrel (e.g., Jencks, 1981), and some results from bilayer-mediated interactions between the two barrels in the double-barreled channels. The increased local concentration will be reflected primarily in the relative appearance rate of the double-barreled channels, which is ~400-fold higher than expected; the bilayer-mediated interactions will be reflected primarily in the relative lifetimes of the double- and single-barreled channels, which is $2 \cdot$ (~400)-fold higher than expected for a simple Poisson process. That is, one can reasonably attribute about half of the increased stabilization, or ~15 kJ/mole, to bilayer-mediated interactions.

Based on $H_B \approx 20$ kJ/(mole $\cdot$ nm^2) and $(d_0 - l) \approx 2$ nm, ΔG^0_{def} for a single-barreled channel in DPhPC/*n*-decane bilayers is ~80 kJ/mole. The bilayer-mediated contribution to the energetic stabilization of the double-barreled channels thus may be ~10% of the bilayer deformation energy associated with having two independent (noninteracting) bilayer-spanning channels. This result is at the same time comforting, because the relative stabilization is rather modest, and surprising, because even this relatively modest stabilization has so dramatic effects on channel function. As noted previously (Durkin et al., 1992), the energetic window for useful perturbations of membrane protein function may be remarkably narrow.

The above analysis leads to the following scheme for the formation of double-barreled channels (Fig. 9).

The linked gramicidins diffuse around in each bilayer leaflet; at some point one subunit from each of

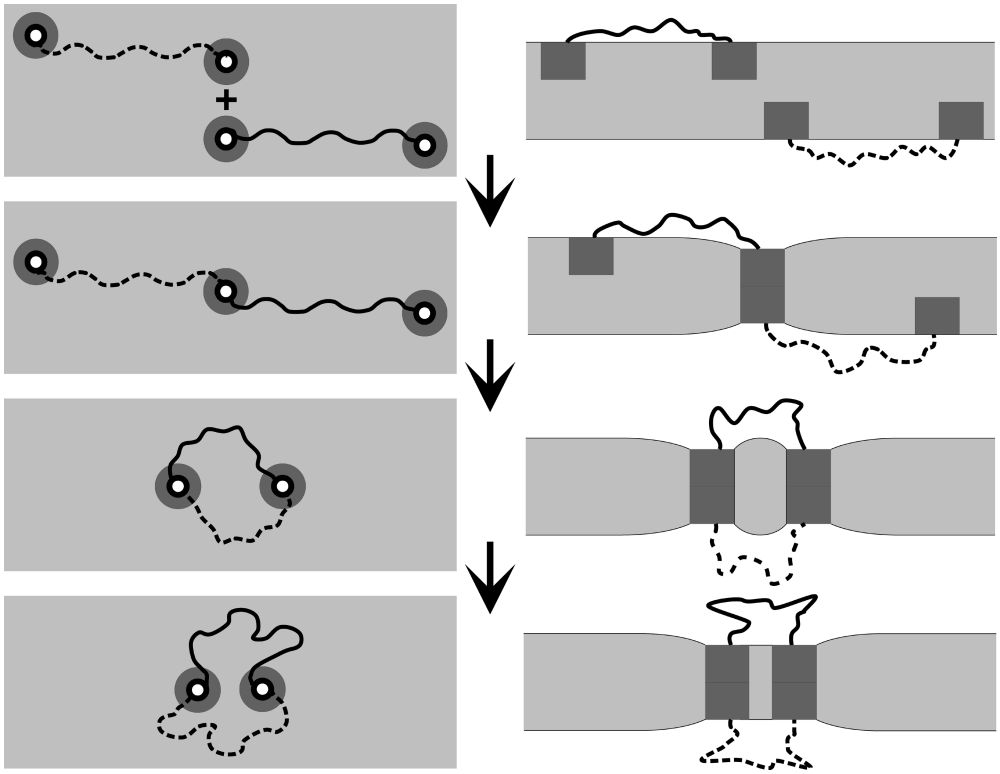

FIGURE 9. Schematic representation of the formation of double-barreled gramicidin channels in a bilayer with a thickness that is larger than the channel length. (Left) top view. (Right) side view. (A) Two independent tandem gramicidins, one on each side of a bilayer, in which the subunits are separated by a flexible linker. (B) The initial event is the formation of a single bilayer-spanning pore with the monomeric subunits at opposite sides of the conducting dimer. The dimerization causes a local thinning of the bilayer around the bilayer-spanning dimer. (C) For the second barrel to form, the subunits diffuse in each monolayer (and the linker bends), causing the nonconducting monomers to approach each other and dimerize, which causes a further bilayer deformation around the second bilayer-spanning dimer. (D) To minimize the overall bilayer deformation energy, the two bilayer-spanning dimers (conducting pores) will tend to associate closely. The figure is drawn with the two barrels separated by a distance corresponding to one phospholipid molecule, but we have no direct information about the distance separating the two barrels.

two linked gramicidins, in opposite leaflets, form a single bilayer-spanning channel (barrel). Then the two "free" subunits diffuse around in the vicinity of this channel, and they form a second barrel, which initially will be relatively independent of the first barrel. But the local bilayer deformation about each barrel will create a driving force to move the two barrels together, to form a "side-by-side" double-barreled channel in which the two barrels may be separated by one phospholipid molecule. This double-barreled channel will be stabilized because the overall bilayer perturbation will be less than twice that imposed by a single bilayer-spanning barrel, such that the balance between stabilizing and destabilizing forces will shift toward greater stabilization. (We do not believe the two barrels are in direct contact, as there is no evidence for lateral association of gA channels in oriented di-lauroyl-phosphatidylcholine bilayers at gA/lipid molar ratios of 1/10 [Harroun et al., 1999a]. Furthermore, gA channels undergo rapid rotational diffusion in solid-state NMR experiments in oriented DMPC bilayers at gA/lipid molar ratios of 1/10 [Lee et al., 1993].)

Why are these interactions seen only in the linked gramicidins? gA single-channel experiments usually are done at gA/lipid ratios $\sim 10^{-7}$ (compare Durkin et al., 1990; Sawyer et al., 1990), corresponding to a subunit density of $\sim 10^{-1}$ μm^{-2} where there is no evidence for interactions between two bilayer-spanning dimers (Cifu et al., 1992). In contrast, the local gA/lipid ratio around a bilayer-spanning channel formed by one of the two subunits in two linked gramicidins would be $2–4 \times 10^{-3}$, more than four orders of magnitude larger than the average subunit density, which would tend to increase the likelihood of subunit interactions. At sufficiently high monomer densities similar interactions should occur if the linked gramicidin were present on only one side of the bilayer and gA on the other, but the unavoidable "leak" of gA across the bilayer (see the histograms in Fig. 8) complicates the detection of these interactions at the single-molecular level. Using macroscopic current relaxations after phtalocyanine-induced photoinactivation, however, Rokitskaya et al. (2003) found that the relaxation time constant indeed increases as the gA concentration increased—consistent with what would be expected at higher gA surface densities.

Together, the results of Rokitskaya et al. (2003) and those of this study provide strong support for the notion that bilayer-spanning inclusions can couple, both structurally and functionally, through the bilayer. The basis for this interaction is likely the bilayer's elastic properties, and the associated bilayer deformation en-

ergy, which could be important for the organization (clustering) of membrane proteins.

Implications for Integral Membrane Proteins

The functions of many membrane proteins depend on the bilayer lipid composition, but usually with only modest chemical specificity in the protein–lipid interactions (Devaux and Seigneuret, 1985; Bienvenüe and Saint-Marie, 1994; Dowhan, 1997; Marsh and Horvath, 1998). Because of the strength of the hydrophobic interactions between the protein's transmembrane domain and the bilayer core, any mismatch between the protein's hydrophobic length and the thickness of the bilayer core will incur an energetic cost that not only may serve to modulate protein function (Brown, 1994; Lundbæk et al., 1996), but also could redistribute/cluster proteins within the bilayer (Pearson et al., 1983; Mouritsen and Bloom, 1984; Gil et al., 1998). This clustering serves to increase the local protein density, which can alter the protein's thermodynamic activity (Ryan et al., 1988) and build up a local stress in the bilayer (Bezrukov, 2000), and thereby modify protein function by altering the energetics, and thus the kinetics, of the cycle of conformational changes associated with protein function.

In any case, the present results demonstrate that adjacent integral membrane proteins can be coupled functionally by the lipid bilayer. The most likely basis for this functional coupling is that the hydrophobic channel–bilayer coupling causes protein conformational changes to perturb the surrounding bilayer, which in turn will later the energetics of conformational changes in neighboring proteins. This shift in the balance between the "intrinsic" energetics of the proteins' conformational changes and the proteins' interactions with their environment, in casu the host bilayer, can alter protein function. To what extent the bilayer-mediated coupling among integral membrane proteins is important for protein function remains to be determined. But ~30% of the cell surface area is occupied by the bilayer-spanning segments of integral membrane proteins, so the local protein density is high, which will facilitate bilayer-mediated protein interactions. In fact, growth factor receptor activation and tyrosine autophosphorylation involve receptor aggregation in the cell membrane (Ullrich and Schlessinger, 1990; Alberts et al., 2002), and caspase-8-dependent apoptosis, which is mediated by death receptors (Saikumar et al., 1999), is activated by amphipathic compounds (Borner et al., 1994; Strupp et al., 2000) that are known to alter bilayer elastic properties (Sawyer et al., 1989). As shown by Rokitskaya et al. (2003), ligand binding can cause gA channels to dimerize, which together with the present results suggest that the hydrophobic coupling between the bilayer and the imbedded proteins may be an important mechanism for regulating the organization and dynamics of membrane proteins.

We thank Drs. Y. Antonenko, P.C. Jordan, M.B. Partenskii, and T. Rokitskaya for helpful discussions and providing unpublished data.

This work was supported by NIH grants GM21342, RR15569, and GM34968, and NSF grant MCB 9816063.

Edward Moczydlowski served as guest editor.

Submitted: 13 January 2003
Revised: 28 March 2003
Accepted: 2 April 2003

REFERENCES

Alberts, B., A. Johnson, J. Lewis, M. Raff, K. Roberts, and P. Walter. 2002. Molecular Biology of the Cell. 4th Edition. Garland Science, New York.

Almers, W., and C. Stirling. 1984. Distribution of transport proteins over animal cell membranes. *J. Membr. Biol.* 77:169–186.

Andersen, O.S. 1978. Ion transport across simple membranes. *In* Renal Function. G.H. Giebisch and E.F. Purcell, editors. The Josiah Macy, Jr. Foundation. 71–99.

Andersen, O.S. 1983a. Ion movement through gramicidin A channels. Single-channel measurements at very high potentials. *Biophys. J.* 41:119–133.

Andersen, O.S. 1983b. Ion movement through gramicidin A channels. Studies on the diffusion-controlled association step. *Biophys. J.* 41:147–165.

Andersen, O.S., D.V. Greathouse, L.L. Providence, M.D. Becker, and R.E. Koeppe II. 1998. Importance of tryptophan dipoles for protein function: 5-fluorination of tryptophans in gramicidin A channels. *J. Am. Chem. Soc.* 120:5142–5146.

Andersen, O.S., C. Nielsen, A.M. Maer, J.A. Lundbæk, M. Goulian, and R.E. Koeppe II. 1999. Ion channels as tools to monitor lipid bilayer-membrane protein interactions: gramicidin channels as molecular force transducers. *Methods Enzymol.* 294:208–224.

Aranda-Espinoza, H., A. Berman, N. Dan, P. Pincus, and S. Safran. 1996. Interaction between inclusions embedded in membranes. *Biophys. J.* 71:648–656.

Baldwin, P.A., and W.L. Hubbell. 1985. Effects of lipid environment on the light-induced conformational changes of rhodopsin. 2. Roles of lipid chain length, unsaturation, and phase state. *Biochemistry.* 24:2633–2639.

Bamberg, E., and P. Läuger. 1973. Channel formation kinetics of gramicidin A in lipid bilayer membranes. *J. Membr. Biol.* 11:177–194.

Becker, M.D., D.V. Greathouse, R.E. Koeppe, II, and O.S. Andersen. 1991. Amino acid sequence modulation of gramicidin channel function. Effects of tryptophan-to-phenylalanine substitutions on the single-channel conductance and duration. *Biochemistry.* 30:8830–8839.

Bezrukov, S.M. 2000. Functional consequences of lipid packing stress. *Curr. Opin. Coll. Interface Sci.* 5:237–243.

Bezrukov, S.M., and I. Vodyanoy. 1993. Probing alamethicin channels with water-soluble polymers. Effect on conductance of channel states. *Biophys. J.* 64:16–25.

Bienvenüe, A., and J. Saint-Marie. 1994. Modulation of protein function by lipids. *Curr. Top. Membr. Transp.* 40:319–354.

Borner, M.M., E. Schneider, F. Pirnia, O. Sartor, J.B. Trepel, and C.E. Myers. 1994. The detergent Triton X-100 induces a death pattern in human carcinoma cell lines that resembles cytotoxic lymphocyte-induced apotosis. *FEBS Lett.* 353:129–132.

Brown, M.F. 1994. Modulation of rhodopsin function by properties of the membrane bilayer. *Chem. Phys. Lipids*. 73:159–180.
Busath, D.D., and G. Szabo. 1981. Gramicidin forms multi-state rectifying channels. *Nature*. 294:371–373.
Chang, E.Y., Y. Zheng, D. Holowka, and B. Baird. 1995. Alteration of lipid composition modulates FcγRI signaling in RBL-2H3 cells. *Biochemistry*. 34:4376–4384.
Cifu, A.S., R.E. Koeppe, II, and O.S. Andersen. 1992. On the supramolecular structure of gramicidin channels. The elementary conducting unit is a dimer. *Biophys. J.* 61:189–203.
Cornea, R., and D.D. Thomas. 1994. Effects of membrane thickness on the molecular dynamics and enzymatic activity of reconstituted Ca-ATPase. *Biochemistry*. 33:2912–2920.
Cornelius, F. 2001. Modulation of Na,K-ATPase and Na-ATPase activity by phospholipids and cholesterol. I. Steady-state kinetics. *Biochemistry*. 40:8842–8851.
Creighton, T.E. 1993. Proteins. Structures and Molecular Properties, 2nd Ed. Freeman, San Francisco, CA.
Devaux, P.F., and M. Seigneuret. 1985. Specificity of lipid-protein interactions as determined by spectroscopic techniques. *Biochim. Biophys. Acta*. 822:63–125.
Dowhan, W. 1997. Molecular basis for membrane phospholipid diversity: why are there so many lipids? *Annu. Rev. Biochem*. 66:199–232.
Durkin, J.T., R.E. Koeppe, II, and O.S. Andersen. 1990. Energetics of gramicidin hybrid channel formation as a test for structural equivalence. Side-chain substitutions in the native sequence. *J. Mol. Biol*. 211:221–234.
Durkin, J.T., L.L. Providence, R.E. Koeppe, II, and O.S. Andersen. 1992. Formation of non-β-helical gramicidin channels between sequence-substituted gramicidin analogues. *Biophys. J.* 62:145–159.
Durkin, J.T., L.L. Providence, R.E. Koeppe, II, and O.S. Andersen. 1993. Energetics of heterodimer formation among gramicidin analogues with an NH_2-terminal addition or deletion. Consequences of a missing residue at the join in channel. *J. Mol. Biol.* 231:1102–1121.
Eisenberg, M., J.E. Hall, and C.A. Mead. 1973. The nature of the voltage-dependent conductance induced by alamethicin in black lipid membranes. *J. Membr. Biol*. 14:143–176.
Elliott, J.R., D. Needham, J.P. Dilger, and D.A. Haydon. 1983. The effects of bilayer thickness and tension on gramicidin single-channel lifetime. *Biochim. Biophys. Acta*. 735:95–103.
Evans, E., and D. Needham. 1987. Physical properties of surfactant bilayer membranes: thermal transitions, elasticity, rigidity, cohesion, and colloidal interactions. *J. Phys. Chem*. 91:4219–4228.
Evans, E.A., and R.M. Hochmuth. 1978. Mechanochemical properties of membranes. *Curr. Top. Membr. Transp*. 10:1–64.
Fanning, A.S., and J.M. Anderson. 1999. Protein modules as organizers of membrane structure. *Curr. Opin. Cell Biol*. 11:432–439.
Fersht, A.R. 1987. The hydrogen bond in molecular recognition. *Trends Biochem. Sci*. 12:301–304.
Gil, T., J.H. Ipsen, O.G. Mouritsen, M.C. Sabra, M.M. Sperotto, and M.J. Zuckermann. 1998. Theoretical analysis of protein organization in lipid membranes. *Biochim. Biophys. Acta*. 1376:245–266.
Goforth, R.L., A.K. Chi, O.S. Andersen, R.E. Koeppe, II, and D.V. Greathouse. 2002. Double-barreled gramicidin channels. *Biophys. J*. 82:557a.
Gordon, L.G.M., and D.A. Haydon. 1972. The unit conductance channel of alamethicin. *Biochim. Biophys. Acta*. 255:1014–1018.
Greathouse, D.V., R.E. Koeppe, II, L.L. Providence, S. Shobana, and O.S. Andersen. 1999. Design and characterization of gramicidin channels. *Methods Enzymol*. 294:525–550.
Harris, A.L. 2001. Emerging issues of connexin channels: biophysics fills the gap. *Q. Rev. Biophys*. 34:325–472.
Harroun, T.A., W.T. Heller, T.M. Weiss, L. Yang, and H.W. Huang. 1999a. Experimental evidence for hydrophobic matching and membrane-mediated interactions in lipid bilayers containing gramicidin. *Biophys. J*. 76:937–945.
Harroun, T.A., W.T. Heller, T.M. Weiss, L. Yang, and H.W. Huang. 1999b. Theoretical analysis of hydrophobic matching and membrane-mediated interactions in lipid bilayers containing gramicidin. *Biophys. J*. 76:3176–3185.
Hladky, S.B., and D.A. Haydon. 1972. Ion transfer across lipid membranes in the presence of gramicidin A. I. Studies of the unit conductance channel. *Biochim. Biophys. Acta*. 274:294–312.
Huang, H.W. 1986. Deformation free energy of bilayer membrane and its effect on gramicidin channel lifetime. *Biophys. J*. 50:1061–1070.
Issa, N.P., and A.J. Hudspeth. 1994. Clustering of Ca^{2+} channels and Ca^{2+}-activated K^+ channels at fluorescently labeled presynaptic active zones of hair cells. *Proc. Natl. Acad. Sci. USA*. 91:7578–7582.
Iwasa, K., G. Ehrenstein, N. Moran, and M. Jia. 1986. Evidence for interactions between batrachotoxin-modified channels in hybrid neuroblastoma cells. *Biophys. J*. 50:531–537.
Jencks, W.P. 1981. On the attribution and additivity of binding energies. *Proc. Natl. Acad. Sci. USA*. 78:4046–4050.
Jordan, P.C. 1986. Ion channel electrostatics and the shapes of channel proteins. *In* Ion Channel Reconstitution. Plenum Press, New York, NY. 37–55.
Kaulin, Y.A., L.V. Schagina, S.M. Bezrukov, V.V. Malev, A.M. Feigin, J.Y. Takemoto, J.H. Teeter, and J.G. Brand. 1998. Cluster organization of ion channels formed by the antibiotic syringomycin E in bilayer lipid membranes. *Biophys. J*. 74:2918–2925.
Koeppe, R.E., II, and O.S. Andersen. 1996. Engineering the gramicidin channel. *Annu. Rev. Biophys. Biomol. Struct*. 25:231–258.
Kusumi, A., and J.S. Hyde. 1982. Spin-label saturation-transfer electron spin resonance detection of transient association of rhodopsin in reconstituted membranes. *Biochemistry*. 21:5978–5983.
Larsen, E.H., S.E. Gabriei, M.J. Stutts, J. Fullton, E.M. Price, and R.C. Boucher. 1996. Endogenous chloride channels of insect Sf9 cells: evidence for coordinated activity of small elementary channel units. *J. Gen. Physiol*. 107:695–714.
Lee, K.C., W. Hu, and T.A. Cross. 1993. 2H NMR determination of the global correlation time of the gramicidin channel in a lipid bilayer. *Biophys. J*. 65:1162–1167.
Lemmon, M.A., and D.M. Engelman. 1994. Specificity and promiscuity in membrane helix interactions. *Q. Rev. Biophys*. 27:157–218.
Lester, H.A. 1977. The response to acetylcholine. *Sci. Am*. 236:106–118.
Levitt, D.G. 1978. Electrostatic calculations for an ion channel. I. Energy and potential profiles and interactions between ions. *Biophys. J*. 22:209–219.
Lewis, B.A., and D.M. Engelman. 1983. Bacteriorhodopsin remains dispersed in fluid phospholipid bilayers over a wide range of bilayer thicknesses. *J. Mol. Biol*. 166:203–210.
Lundbæk, J., and O.S. Andersen. 1999. Spring constants for channel-induced lipid bilayer deformations - estimates using gramicidin channels. *Biophys. J*. 76:889–895.
Lundbæk, J.A., P. Birn, J. Girshman, A.J. Hansen, and O.S. Andersen. 1996. Membrane stiffness and channel function. *Biochemistry*. 35:3825–3830.
Manivannan, K., S.V. Ramanan, R.T. Mathias, and P.R. Brink. 1992. Multichannel recordings from membranes which contain gap junctions. *Biophys. J*. 61:216–227.
Marsh, D., and L.I. Horvath. 1998. Structure, dynamics and composition of the lipid-protein interface. Perspectives from spin-labeling. *Biochim. Biophys. Acta*. 1376:267–296.

Marx, S.O., K. Ondrias, and A.R. Marks. 1998. Coupled gating between individual skeletal muscle Ca^{2+} release channels (ryanodine receptors). *Science.* 281:818–821.

Mergler, M., R. Tanner, J. Gosteli, and P. Grogg. 1988. Peptide synthesis by a combination of solid-phase and solution methods I: A new very acid-labile anchor group for solid-phase synthesis of fully protected fragments. *Tetrahedron Lett.* 29:4005–4008.

Mobashery, N., C. Nielsen, and O.S. Andersen. 1997. The conformational preference of gramicidin channels is a function of lipid bilayer thickness. *FEBS Lett.* 412:15–20.

Mouritsen, O.G., and O.S. Andersen. 1998. In search of a new biomembrane model. *Biol. Skr. Dan. Vid. Selsk.* 49.

Mouritsen, O.G., and M. Bloom. 1984. Mattress model of lipid-protein interactions in membranes. *Biophys. J.* 46:141–153.

Neumcke, B., and R. Stämpfli. 1983. Alteration of the conductance of Na^+ channels in the nodal membrane of frog nerve by holding potential and tetrodotoxin. *Biochim. Biophys. Acta.* 727:177–184.

Nielsen, C., M. Goulian, and O.S. Andersen. 1998. Energetics of inclusion-induced bilayer deformations. *Biophys. J.* 74:1966–1983.

Nielsen, C., and O.S. Andersen. 2000. Inclusion-induced bilayer deformations: effects of monolayer equilibrium curvature. *Biophys. J.* 79:2583–2604.

Olah, G.A., H.W. Huang, W. Liu, and Y. Wu. 1991. Location of ion-binding sites in the gramicidin channel by x-ray diffraction. *J. Mol. Biol.* 218:847–858.

Parsegian, A. 1969. Energy of an ion crossing a low dielectric membrane: Solutions to four relevant electrostatic problems. *Nature.* 221:844–846.

Partenskii, M.B., and P.C. Jordan. 2002. Membrane deformation and the elastic energy of insertion: Perturbation of membrane elastic constants due to peptide insertion. *J. Chem Phys.* 117: 10768–10776.

Pearson, L.T., S.I. Chan, B.A. Lewis, and D.M. Engelman. 1983. Pair distribution functions of bacteriorhodopsin and rhodopsin in model bilayers. *Biophys. J.* 43:167–174.

Poo, M.M. 1985. Mobility and localization of proteins in excitable membranes. *Annu. Rev. Neurosci.* 8:369–406.

Popot, J.L., and D.M. Engelman. 1990. Membrane protein folding and oligomerization: The two-stage model. *Biochemistry.* 29:4031–4037.

Redwood, W.R., F.R. Pfeiffer, J.A. Weisbach, and T.E. Thompson. 1971. Physical properties of bilayer membranes formed from a synthetic saturated phospholipid in n-decane. *Biochim. Biophys. Acta.* 233:1–6.

Roberts, W.M., R.A. Jacobs, and A.J. Hudspeth. 1990. Colocalization of ion channels involved in frequency selectivity and synaptic transmission at presynaptic active zones of hair cells. *J. Neurosci.* 10:3664–3684.

Rokitskaya, T.I., Y.N. Antonenko, and E.A. Kotova. 1996. Photodynamic inactivation of gramicidin channels: a flash-photolysis study. *Biochim. Biophys. Acta.* 1275:221–226.

Rokitskaya, T.I., E.A. Kotova, and Yu.N. Antonenko. 2003. Tandem gramicidin channels cross-linked by streptavidin. *J. Gen. Physiol.* 121:463–476.

Ryan, T.A., J. Myers, D. Holowka, B. Baird, and W.W. Webb. 1988. Molecular crowding on the cell surface. *Science.* 239:61–64.

Saikumar, P., Z. Dong, V. Mikhailov, M. Denton, J. Weinberg, and M.A. Venkatachalam. 1999. Apoptosis: definition, mechanisms, and relevance to disease. *Am. J. Med.* 107:489–506.

Sawyer, D.B., R.E. Koeppe, II, and O.S. Andersen. 1989. Induction of conductance heterogeneity in gramicidin channels. *Biochemistry.* 28:6571–6583.

Sawyer, D.B., R.E. Koeppe, II, and O.S. Andersen. 1990. Gramicidin single-channel properties show no solvent-history dependence. *Biophys. J.* 57:515–523.

Schulz, G.E., and R.H. Schirmer. 1979. Principles of Protein Structure. Springer-Verlag, New York.

Sigworth, F.J., and S. Shenkel. 1988. Rapid gating events and current fluctuations in gramicidin A channels. *Curr. Top. Membr. Transp.* 33:113–130.

Simons, K., and E. Ikonen. 1997. Functional rafts in cell membranes. *Nature.* 387:569–572.

Singer, S.J., and G.L. Nicolson. 1972. The fluid mosaic model of the structure of cell membranes. *Science.* 175:720–731.

Starling, A.P., J.M. East, and A.G. Lee. 1995. Evidence that the effects of phospholipids on the activity of the Ca^{2+}-ATPase do not involve aggregation. *Biochem. J.* 308:343–346.

Strupp, W., G. Weidinger, C. Scheller, R. Ehret, H. Ohnimus, H. Girschick, P. Tas, E. Flory, M. Heinkelein, C. Jassoy. 2000. Treatment of cells with detergent activates caspases and induces apoptotic cell death. *J. Membr. Biol.* 175:181–189.

Tkachenko, E., and M. Simons. 2002. Clustering induces redistribution of syndecan-4 core protein into raft membrane domains. *J. Biol. Chem.* 277:19946–19951.

Ullrich, A., and J. Schlessinger. 1990. Signal transduction by receptors with tyrosine kinase activity. *Cell.* 61:203–212.

Veatch, W.R., R. Mathies, M. Eisenberg, and L. Stryer. 1975. Simultaneous fluorescence and conductance studies of planar bilayer membranes containing a highly active and fluorescent analog of gramicidin A. *J. Mol. Biol.* 99:75–92.

Veprek, P., and J. Jezek. 1999. Peptide and glycopeptide dendrimers. II. *J. Pept. Sci.* 5:203–220.

White, S.H., and W.C. Wimley. 1999. Membrane protein folding and stability: physical principles. *Annu. Rev. Biophys. BioMol. Struct.* 28:319–365.

Woolley, G.A., V. Zunic, J. Karanicolas, A.S. Jaikaran, and A.V. Starostin. 1997. Voltage-dependent behavior of a "ball-and-chain" gramicidin channel. *Biophys. J.* 73:2465–2475.

Young, S.H., and M.M. Poo. 1983. Topographical rearrangement of acetylcholine receptors alters channel kinetics. *Nature.* 304:161–163.